

Contribution of Face and Core Layers to Lateral Load Resistance of Single-Shear Metal-to-Particleboard Single-Screw Connections

Yan Wang ^a and Jilei Zhang ^{b,*}

The lateral load-slip behavior of a single-shear metal-to-particleboard single-screw connection (SMPSC) was investigated. The connection consisted of a layered particleboard main member fastened to a metal plate as a side member using a 4.8-mm diameter sheet metal screw. A mechanics-based approach was used to evaluate critical factors on the lateral load resistance performance of SMPSCs. Experimental results indicated that ultimate screw-bearing strengths in face and core layers of evaluated particleboard materials were 100.0 and 29.9 MPa, respectively. This significant difference of screw-bearing strength in material layers significantly affected the lateral resistance load capacity of SMPSCs. The proposed mechanical models considering material layer effects on screw-bearing strengths were verified experimentally as a valid means for deriving estimation equations of lateral resistance loads of SMPSCs evaluated in this study.

Keywords: Single shear screwed connections; Lateral load resistance; Particleboard; Screw bending moment; Screw-bearing strength; Yield theory

Contact information: a: Academy of Design & Art, Hunan Institute of Engineering, Xiangtan 411104, China. Former PhD Student, Department of Sustainable Bioproducts, Mississippi State University; b: Department of Sustainable Bioproducts, Mississippi State University, P. O. Box 9680, MS 39762-9820; * Corresponding author: jz27@msstate.edu

INTRODUCTION

Particleboard (PB) is commonly produced from various sizes of wood particles through applying thermosetting adhesive to the particles and pressing a loose mat of the particles with heat and pressure (Williamson 2002). The consumption of PB is mainly in furniture manufacturing (UNECE 2016), especially in the cabinet industry because of its good strength properties, smooth surfaces, and low price. A single-shear metal-to-particleboard single-screw connection (SMPSC) is commonly seen in jointing door hinges to PB structural components in cabinet construction. Therefore, knowing the lateral load resistance capacity of a SMPSC can provide fundamental information in assisting the strength design of cabinets constructed of PB.

Previous studies related to lateral resistance load capacities of single-shear mechanical fastener wood-to-wood connections (Blaß and Bejtka 2002; Hansen 2002; Taj *et al.* 2009;) and metal-to-wood (Aune and Patton-Mallory 1986; Hunt and Bryant 1990; Chui *et al.* 2006) or wood-based composite connections (Karacabeyli *et al.* 1998; Sinha and Byrne 2013; Kuang *et al.* 2017; Yu *et al.* 2017) considered a main member as a homogenous material, *i.e.*, assuming that the dowel-bearing strength of the material underneath the dowel is the same (Soltis *et al.* 1986).

PB is typically made in layers. The faces of PB usually consist of fine particles, while the core is made up of coarser ones. Normally, a symmetrical “U”-shape density profile across the panel thickness, *i.e.*, face layers have higher density than core material, will be developed during the mat forming and hot processing process. This density profile across the PB panel thickness can lead to the face layer material having higher mechanical properties, such as dowel-bearing strength, than the core. Karacabeyli *et al.* (1998) indicated that glulam rivet connections constructed of low density spruce-pine-fir and hemlock-fir were 5% and 25% lower in lateral capacity than high density Douglas-fir-larch.

The main objective of this study was to develop prediction equations for lateral resistance loads of SMPSCs. The specific objectives were to 1) evaluate screw-bearing strengths of PB materials; 2) characterize the lateral load-slip behavior and failure mode of SMPSCs; 3) propose mechanical models based on the screw and PB member failure modes for describing the internal force distribution in the connection at different loading stages; 4) derive equations based on proposed mechanical models for predicting lateral resistance loads of SMPSCs at different loading stages; and 5) validate derived prediction equations experimentally.

EXPERIMENTAL

Materials

In this study, full-sized four-layers M-2 Grade (ANSI A208.1 2016.) PB panels provided by Roseburg Particleboard Company (Taylorsville, MS, USA), measured 2,464-mm long \times 1,245-mm wide \times 28.6-mm thick, were used. The grade #4140, 3.3-mm thick alloy steel metal plate was purchased from McMaster-Carr Company (Douglasville, GA, USA). The #10 Phillips flat head sheet metal screws (Table 1 and Fig. 1) were purchased from the Hillman Group Company (Cincinnati, OH, USA).

Table 1. Sheet Metal Screw Critical Dimensions

	Total Length (mm)	Thread Length (mm)	Tip Length (mm)	Major Diameter (mm)	Root Diameter (mm)
Product dimensions	38.1	35.2	---	4.8	---
Actual dimensions	37.5 (0.4)	32.9 (0.3)	3.7 (0.2)	4.8 (0.3)	3.6 (0.3)

Note: Values in parentheses are coefficients of variation in percentage.

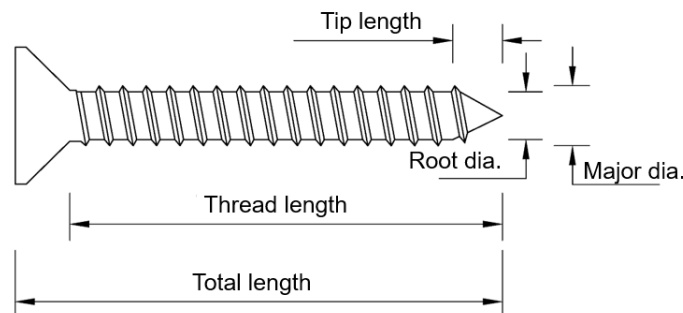


Fig. 1. The general configuration of a sheet metal screw with critical dimensions.

Experimental Design

Screw connections

The general configuration of a SMPSC used in this study is shown in Fig. 2. The connection consisted of a PB main member attached to a metal-plate side member through a single screw. The PB main member measured 101.6-mm long \times 254.0-mm wide \times 28.6-mm thick according to ASTM D1761 (2012). The metal-plate side member measured 228.6-mm long \times 88.9-mm wide \times 3.3-mm thick. 15 replicates of SMPSCs were tested. In addition, three replicates of SMPSCs were loaded to each of five averaged deformation levels (0.76, 1.27, 2.54, 3.81, and 5.08 mm) to investigate how the joint failure progressed in terms of when the PB material started being crushed and when the screw started being bent.

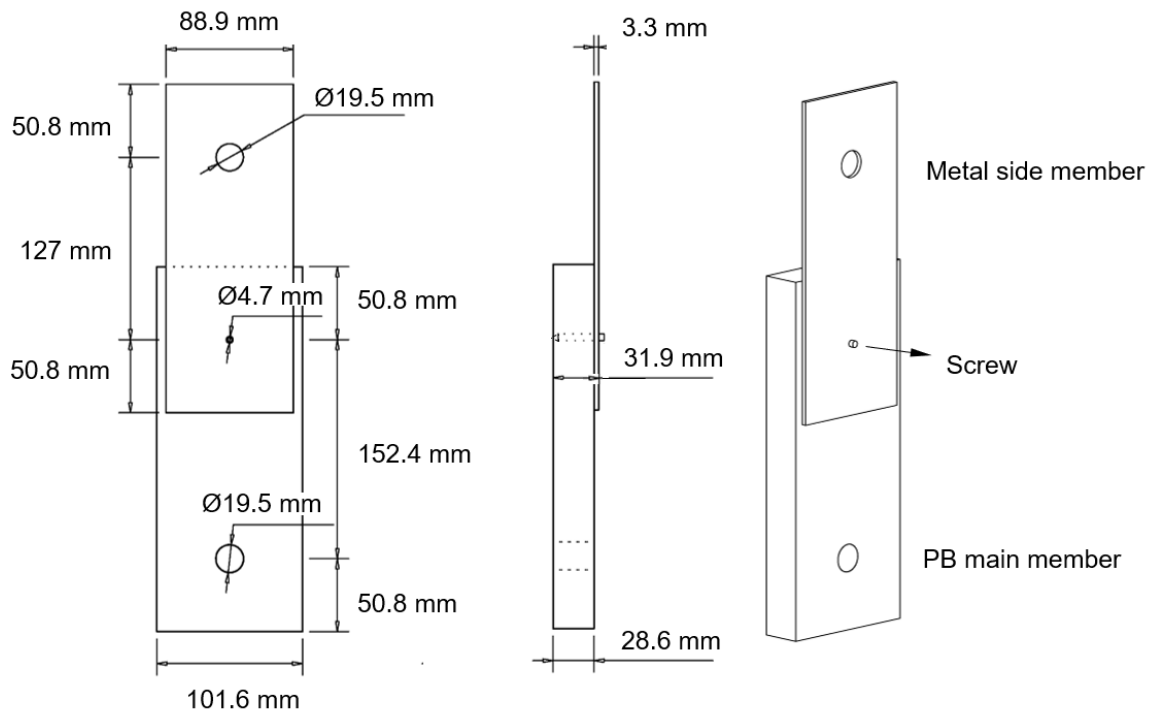


Fig. 2. The general configuration of a SMPSC: front view, side view, and 3D view.

Basic material properties

Figure 3a shows the general configuration of a half-hole specimen used for evaluating screw-bearing strengths in PB materials. The specimen measured 76.2-mm long \times 76.2-mm wide with a 3.3-mm diameter half-hole drilled through board thickness ASTM D5764 (2018). Figure 3b shows three specific types of specimens cut for evaluating screw-bearing strengths in full thickness PB, face layers, and core layer. Cutting to prepare layers from which to assemble the core and face specimens was done with a band saw. The replicates were 27, 36, and 36 for full thickness PB, core layer, and face layer specimens, respectively. Bending properties of 20 randomly selected screws were tested according to ASTM F1575 (2017). 15 replicates specific gravity (SG) and moisture content (MC) of PB materials measured 50.8-mm long \times 50.8-mm wide \times 28.6-mm thick were tested according to ASTM D2395 (2017) and ASTM D4442 (2013), respectively.

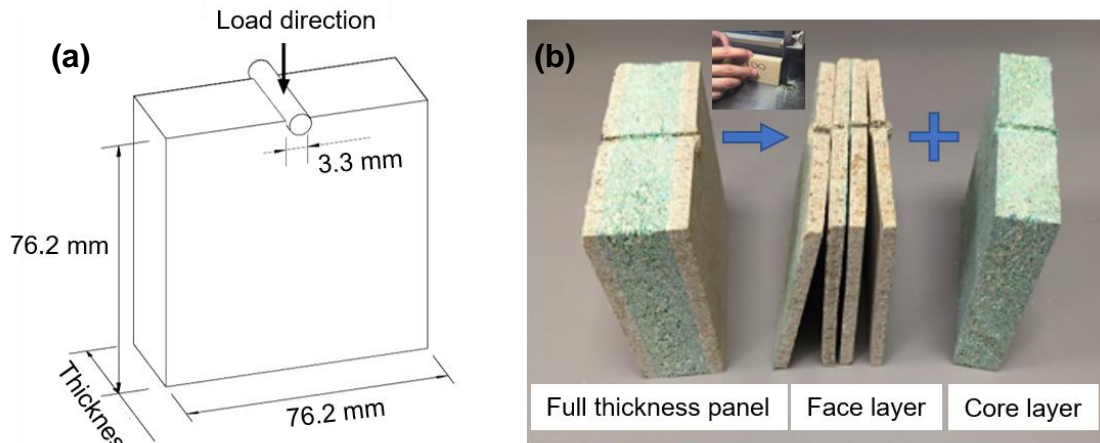


Fig. 3. The general configuration of (a) a half-hole specimen used for evaluating screw-bearing strengths in particleboard and (b) three specific types of specimens cut for evaluating screw-bearing strengths in full thickness PB, face layer, and core layer.

Specimen Preparation and Testing

Figure 4 shows the cutting pattern for preparing the screw-bearing strength specimens. Particularly, the core layer material was dyed with a green color during the manufacturing process. Four sliced face layers of PB materials, each measuring 4.57 mm, were clamped together as one face layer specimen measured 18.28 mm in its thickness. The core layer specimen thickness measured 20 mm. All PB main members were randomly cut from the rest of leftover sections after the preparation of screw-bearing strength specimens. Prior to testing, all specimens were conditioned in an environmental humidity chamber controlled at 20 ± 2 °C and at $50 \pm 5\%$ relative humidity for 40 h. The SG and MC samples were cut from each tested main member.

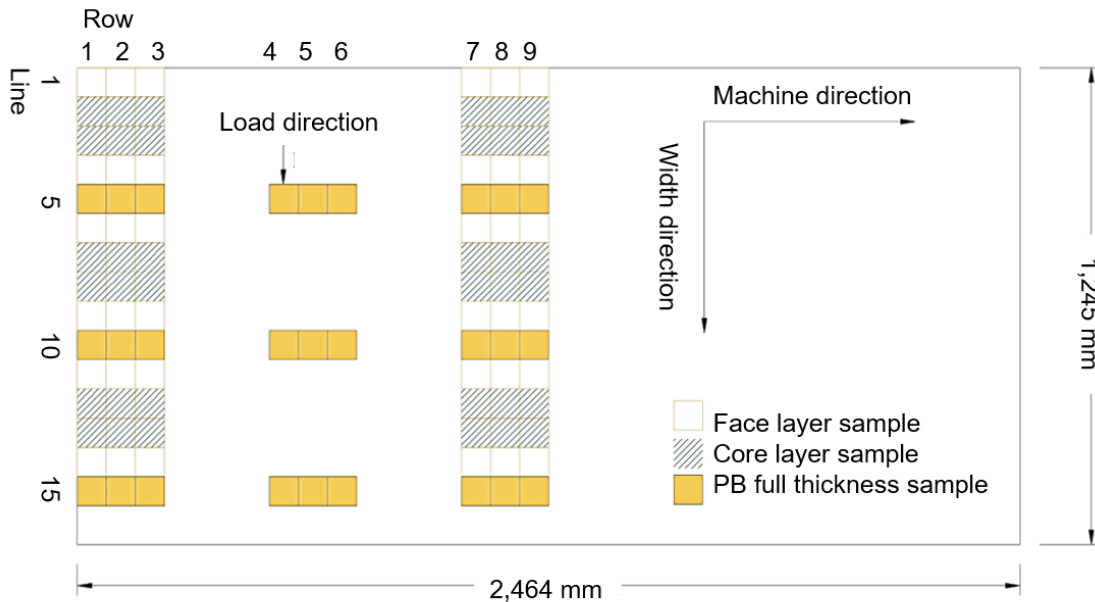


Fig. 4. Cutting pattern used for preparing screw-bearing strength specimens.

All screw-bearing, screw-bending, and connection tests were performed on a hydraulic SATEC universal testing machine purchased from INSTRON company,

(Norwood, MA, USA). Figure 5a shows the setup for evaluating the lateral resistance load-slip behavior of a SMPSC. The screw-driving torque was set to 2.8 N-m (Tor *et al.* 2015). A linear variable differential transformer (LVDT) electromagnetic device was attached on the PB main member to measure the connection slip. The loading speed was 1.0 mm/min ASTM D1761 (2012). Figure 5b shows the details of how the two metal plates were attached to the PB main member for specimens tested for the investigation of connection failure progress. Two metal pieces were attached to the main member; by such means these two metal plates could be removed after the tested connection reached the desired slip. The bent shape of a tested screw was examined using an INSPEX X-ray inspection system purchased from KODEX company (Nutley, NJ, USA).

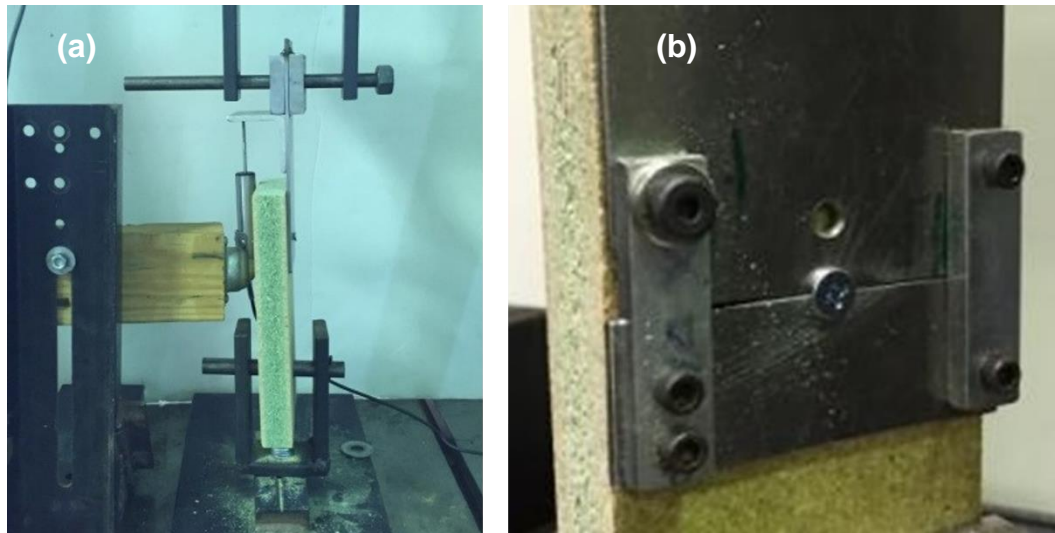


Fig. 5. Test setups for evaluating the lateral load-slip behavior of a single-shear metal-to-particleboard single-screw connection using (a) one metal piece and (b) two removable metal pieces as the side member, respectively

Figure 6 shows the setup for evaluating half-hole screw-bearing strength properties in PB materials.



Fig. 6. Test setup for evaluating half-hole screw-bearing strength properties in particleboard

The screw was compressed into a half-hole PB specimen with a constant rate of 1 mm/min ASTM D5764 (2018). The critical screw-bearing strength values at proportional limit ($F_{e,o,pl}$), 5% offset yield ($F_{e,o,y}$), and ultimate ($F_{e,o,u}$) for PB in board thickness; screw-bearing strength values at proportional limit ($F_{e,c,pl}$), 5% offset yield ($F_{e,c,y}$), and ultimate ($F_{e,c,u}$) for PB core layer; and screw-bearing strength values at proportional limit ($F_{e,f,pl}$), 5% offset yield ($F_{e,f,y}$), and ultimate ($F_{e,f,u}$) for PB face layer materials, were calculated using Eq. 1,

$$F_e = P/dt \quad (1)$$

where F_e is the characteristic screw-bearing strength (MPa); P is the compressive load (N); d is the screw thread diameter (mm); and t is the thickness of a PB specimen (mm).

Figure 7 shows the setup for evaluating the bending moment of screws used in this study. The center-loading bending test at a constant displacement rate of 6.35 mm/min was implemented with a span of 22.9 mm, ASTM F1575 (2017). The critical bending moments of M_{pl} at proportional limit, M_y at yield point, and M_u at ultimate point (N-mm) were calculated using Eq. 2,

$$M = P_b S_{bp}/4 \quad (2)$$

where P_b is the test bending load at each critical point as determined from load-displacement curves (N); and S_{bp} is the span between two supports (mm).



Fig. 7. Setup for evaluating the bending moment capacity of screws

Load-slip curves and failure modes of all tested connections were recorded. The yield load of a tested connection was determined through fitting a straight line to the initial linear portion of the load-slip curve recorded, offsetting this line by a slip equal to 5% of the screw major diameter.

RESULTS AND DISCUSSION

Basic Physical and Mechanical Properties

PB SG averaged 0.7 with a coefficient of variation (COV) of 5.0 % and PB MC averaged 7.0% with a COV) of 4.1% based on 15 replicates. Figure 8 shows a typical bending moment-displacement curve of screw bending strength tests. The mean values with their COVs of screw bending moments at proportional limit, M_{pl} ; at yield point, M_y ;

at ultimate point, M_u ; were 11,190 (2.1%), 12,659 (1.9%), and 13,338 (2.8%) N-mm, respectively.

Figure 9 shows typical load-embedment curves of screw-bearing strength tests performed in face layer, core layer, face and full thickness PB, respectively. Table 2 summarizes mean values of screw-bearing strengths in different layers of PB materials, including their values at proportional limit, yield point, and ultimate point for face layer, core layer, and full thickness PB, respectively. Mean comparisons among three values within each strength value column were performed at the 5% significance level using the protected least significant difference (LSD) multiple comparison procedure, *i.e.*, LSD values were 3.0, 2.9, and 2.88 MPa for proportional limit, yield, and ultimate strengths, respectively.

Mean comparison results indicated that in general, there were significant differences in screw-bearing strengths among three different layered materials evaluated. In other words, screw-bearing strengths in face layer materials were significantly higher than those in full thickness PB, followed by those in core materials.

Table 2. Mean Value of Screw-Bearing Strength Properties in Particleboards

Layer Type	Proportional Limit (MPa)	Yield (MPa)	Ultimate (MPa)
Face	$F_{e,f,pl} = 90.2 (11)^a A^b$	$F_{e,f,y} = 94.5 (10) A$	$F_{e,f,u} = 100.0 (9) A$
Core	$F_{e,c,pl} = 26.5 (10) B$	$F_{e,c,y} = 28.2 (10) B$	$F_{e,c,u} = 29.9 (9) B$
full thickness PB	$F_{e,o,pl} = 51.6 (6) C$	$F_{e,o,y} = 54.4 (6) C$	$F_{e,o,u} = 58.8 (5) C$

Note: Values in parentheses are coefficients of variation in percentage. Means in each column not followed by a common letter are significantly different from one another at the 5% significance level.

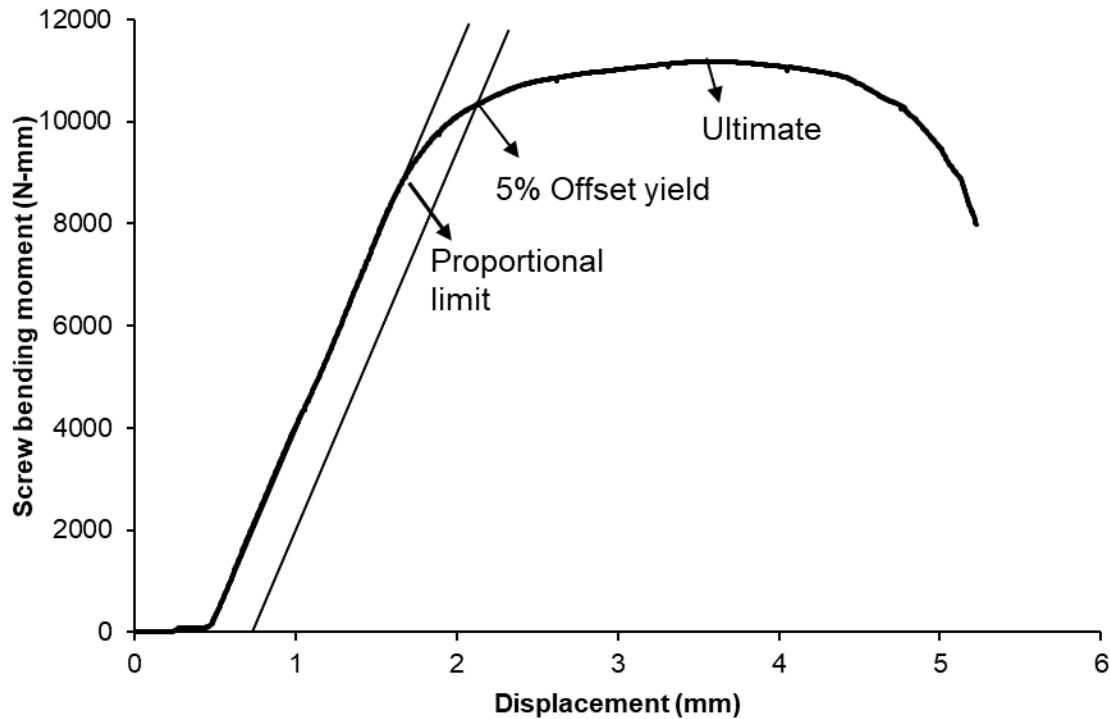


Fig. 8. A typical bending moment-displacement curve of tested screws

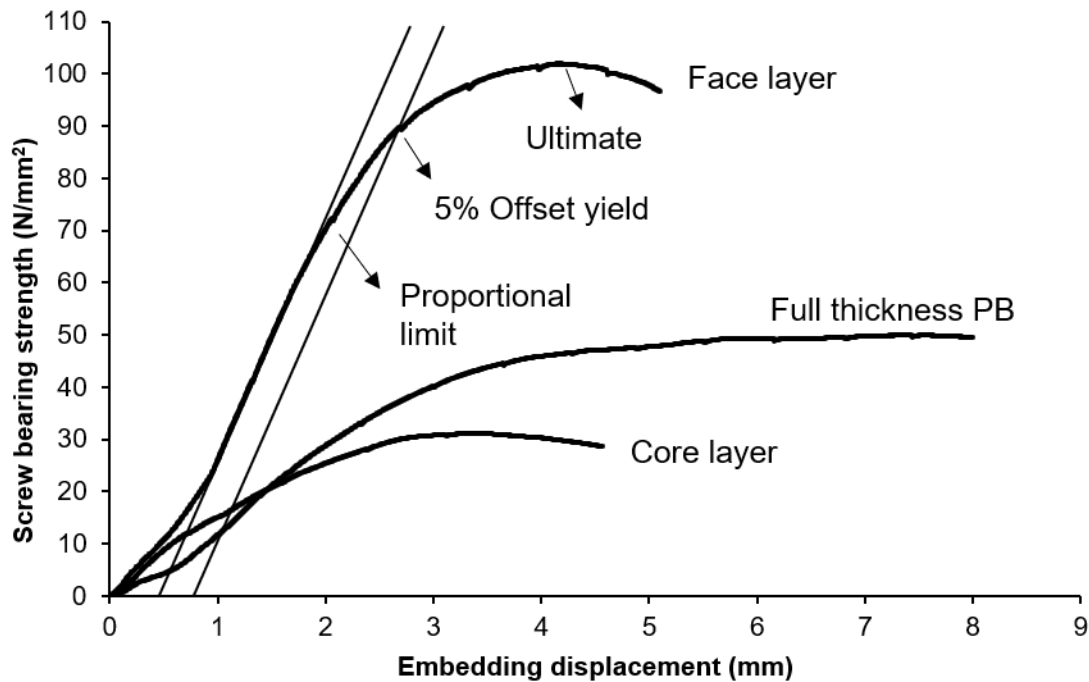


Fig. 9. Typical bearing strength-embedding displacement curves of screws tested in face layer, core layer, and full thickness PB of evaluated particleboard materials

Screwed Connections

Load-slip curves and failure modes

Figure 10 is a typical load-slip curve of SMPSCs when subjected to a lateral load, having three different stages. Stage 1 started from the first linear-elastic line to the first offset yield point. The linear portion of Stage 1 was because of PB material underneath the screw was compressed in its elastic region and there was no sign of the screw being bent (Fig. 11a) as the lateral load increased from 0 to 1,560 N. There was an initial linear-yield portion up to a specific load level (1,870 N in this curve) where the yield portion was mainly because of the screw having a slight one-point bent (Fig. 11b) at the PB-to-metal contact surface. In other words, one plastic hinge was developed, rather than fractured PB materials because there was not any obvious compressive fracture having occurred at PB material underneath the screw (Fig. 11a and b).

Stage 2 is the second linear-yield portion (Fig. 10), which started from the first offset yield point to the second offset yield point. In this stage, the PB material moved its deformation transition from elastic to plastic, *i.e.*, the linear portion up to a lateral load level (3,110 N) means that the PB material underneath the screw was still in its elastic region, and further increasing the load fractured the PB material underneath the screw (Fig. 11c and d). Meanwhile, the screw started its two-point bending process (Fig. 11c) when the lateral load reached a level (3,110 N), *i.e.*, the second screw plastic hinge appeared in the inner section of the PB, and two plastic hinges (Fig. 11d) were developed as the load increased to the second yield loading point (3,780 N).

In Stage 3 the lateral load started from the second offset yield point, reached its maximum value (Fig. 11e) at a slip level (5 mm), and then dropped gradually. In this stage, the screw continued its two plastic hinge bending process (Fig. 11e), started its pulling-out process, and ended with screw head broken off (Fig. 11f), while the PB material underneath the screw continued its compressed-yielding process (Fig. 10e). The screw started its pulling-out when the lateral load reached its maximum (Fig. 11e and f).

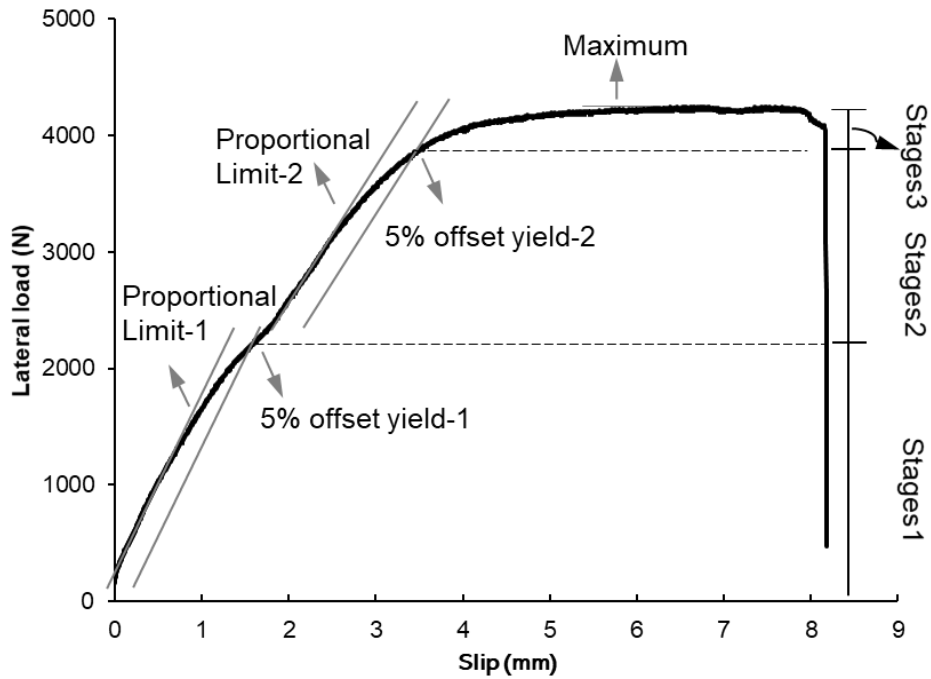


Fig. 10. A typical lateral load-slip curve of single-shear metal-to-particleboard single-screw connections

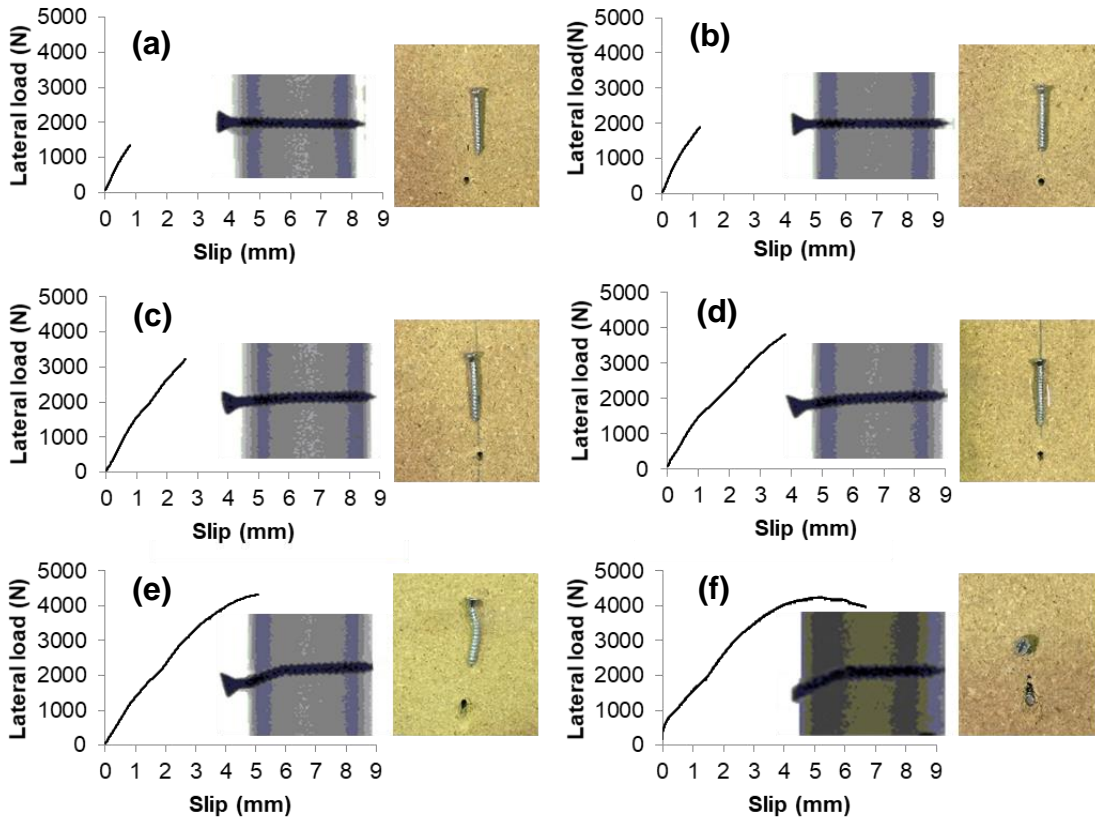


Fig. 11. Showing load-slip curves recorded on single-shear metal-to-particleboard single-screw connections when loaded to six slip levels of: (a) 0.76 mm, (b) 1.27 mm, (c) 2.54 mm, (d) 3.81 mm, (e) 5.08 mm, and (f) screw head broken off, respectively together with their corresponding X-ray images showing screw bent shapes and photos showing actual screw bent and PB material fractured compressively

Linear models

Figure 12 shows proposed linear mechanical models, including their free-body diagrams of the portion of a screw in the main member, for the derivation of prediction equations of lateral resistance loads of SMPSCs at their proportional limits in Stage 1 (Fig. 10). Specifically, Model I-a (Fig. 12a) considers PB as a uniform material across its thickness with a same screw-bearing strength across PB thickness, while Model I-b (Fig. 12b) considers PB as a layered material with different screw-bearing strengths in its core and face materials, respectively. The assumptions made based on failure modes observed (Fig. 11a) are that 1) PB material in compression beneath the screw is in its elastic range because no obvious non-recoverable deformation was observed at this stage; 2) the compression end close to the metal plate, point A, reaches its unit screw-bearing load at proportional limit, $F_{e,o,pl} d$ (N/mm), for Model I-a, and point C just reaches its unit screw-bearing yield load in core materials, $F_{e,c,y} d$ (N/mm) for Model I-b; and 3) the screw bends in its elastic range. The bending moment at point A just reaches its value, M_{pl} (N-mm), at the proportional limit.

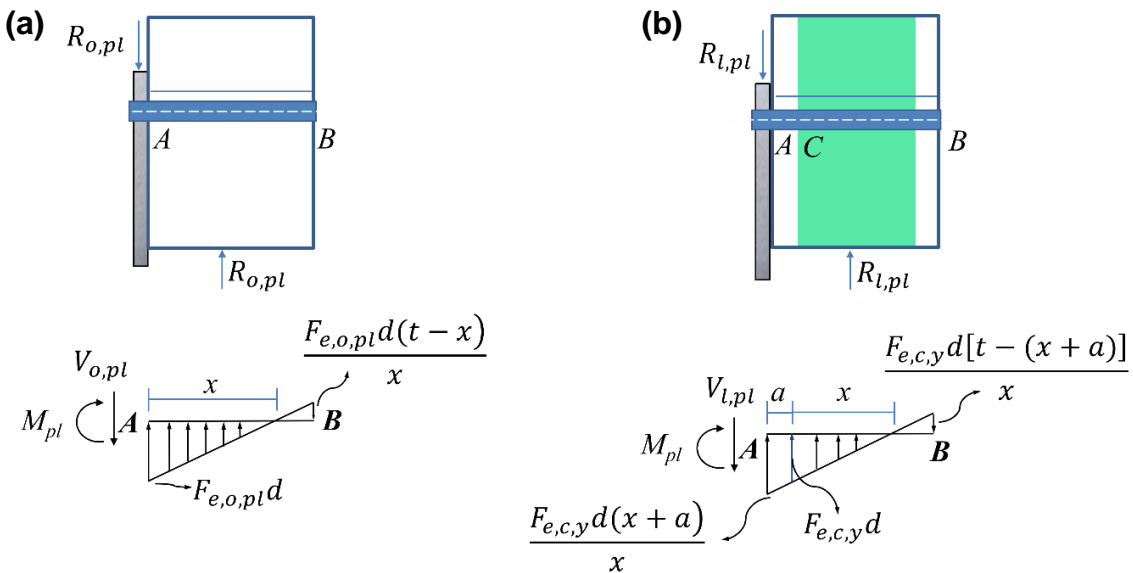


Fig. 12. Mechanical schematic diagrams for linear model (a) Model I-a and (b) Model I-b

Based on the geometric relationship of Model I-a (Fig. 12a), the bearing unit load at point B can be derived as $\frac{F_{e,o,pl}d(t-x)}{x}$. Summarizing all moments to zero at pivot point A yields the moment equation (Eq. 3).

$$M_{pl} + \left[\frac{(t-x) \frac{F_{e,o,pl}d(t-x)}{2}}{2} \right] \left[x + \frac{2(t-x)}{3} \right] - \left(\frac{x F_{e,o,pl}d}{2} \right) \left(\frac{x}{3} \right) = 0 \quad (3)$$

Summarizing all forces in the vertical direction to zero yields the vertical force equation (Eq. 4).

$$V_{o,pl} - \frac{1}{2} F_{e,o,pl} dx + \frac{1}{2} F_{e,o,pl} (t-x) = 0 \quad (4)$$

Solving the above two equations yields the equation for calculation of the

proportional limit shear force at Stage 1, $V_{o,pl}$ (N), at point A of the screw (Eq. 5).

$$V_{o,pl} = -\frac{1}{2}F_{e,o,pl}d \frac{2F_{e,o,pl}dt^3}{3(F_{e,o,pl}dt^3 - 2M_{pl})} + \frac{1}{2}F_{e,o,pl} \left(t - \frac{2F_{e,o,pl}dt^3}{3(F_{e,o,pl}dt^3 - 2M_{pl})} \right) \quad (5)$$

By setting $k_1 = \frac{2F_{e,o,pl}dt^3}{3(F_{e,o,pl}dt^3 - 2M_{pl})}$ and $R_{o,pl} = V_{o,pl}$, the lateral resistance load of SMPSCs, $R_{o,pl}$ (N), at proportional limit in stage 1 can be estimated using the following equation based on Model I-a.

$$R_{o,pl} = \frac{1}{2}F_{e,o,pl}[(t + (d - 1)k_1)] \quad (6)$$

Based on the geometric relationship of Model I-b (Fig. 12b), the bearing unit loads at points A and B can be derived as $\frac{F_{e,c,y}d(x+a)}{x}$ and $\frac{F_{e,c,y}d[t-(x+a)]}{x}$, respectively. Summarizing all moments to zero at pivot point A yields the moment equation (Eq. 7).

$$M_{pl} + \frac{[t-(x+a)] \frac{F_{e,c,y}d[t-(x+a)]}{x}}{2} \left[(x+a) + \frac{2[t-(x+a)]}{3} \right] - \frac{(x+a) \frac{F_{e,c,y}d(x+a)}{x}}{2} \frac{x+a}{3} = 0 \quad (7)$$

Summarizing all forces in the vertical direction to zero yields the vertical force equation (Eq. 8).

$$V_{l,pl} - \frac{1}{2} \frac{F_{e,c,y}d(x+a)}{x} (x+a) + \frac{1}{2} [t-(x+a)] \frac{F_{e,c,y}d[t-(x+a)]}{x} = 0 \quad (8)$$

Solving above two equations yields the following equation for calculation of the proportional limit shear force at Stage 1, $V_{l,pl}$ (N), at point A of the screw (Eq. 9).

$$V_{l,pl} = \frac{F_{e,c,y}d \left[-\frac{F_{e,c,y}dt^2(3a-2t)}{3(df t^2 - 2M_{pl})} + a \right]^2}{2x} - \frac{F_{e,c,y}d \left[t - \left(-\frac{F_{e,c,y}dt^2(3a-2t)}{3(df t^2 - 2M_{pl})} + a \right) \right]^2}{2x} \quad (9)$$

By setting $k_2 = -\frac{F_{e,c,y}dt^2(3a-2t)}{3(df t^2 - 2M_{pl})} + a$ and $R_{l,pl} = V_{l,pl}$, the lateral resistance load of SMPSCs, $R_{l,pl}$ (N), at proportional limit in stage 1 can be estimated using the following equation based on Model I-b (Eq. 10).

$$R_{l,pl} = \frac{F_{e,c,y}d(2tk_2 - t^2)}{2x} \quad (10)$$

Figure 13 shows proposed linear mechanical models for the derivation of prediction equations of lateral resistance loads of SMPSCs at their 5% offset yield points at Stage 1 (Fig. 10). Specifically, Model II-a (Fig. 13a) considers PB as a uniform material across its thickness, while Model II-b (Fig. 13b) considers PB as a layered material with different screw-bearing strengths in core and face materials, respectively. The assumptions made based on the failure modes observed (Fig. 11a and b) are that 1) PB material in compression beneath the screw is in its elastic range because no obvious non-recoverable deformation was observed at this stage; 2) the compression end close to the metal plate, point A, reaches its screw-bearing strength at proportional limit, $F_{e,o,pl}$ (N/mm) for Model II-a. Point C reaches its core material screw-bearing strength at yield, $F_{e,c,y}d$ (N/mm) for Model II-b because of its lower screw-bearing strength if compared to face material; and 3) the screw starts to bend, just reaches its yield bending moment, M_y (N-mm), and remains in static equilibrium.

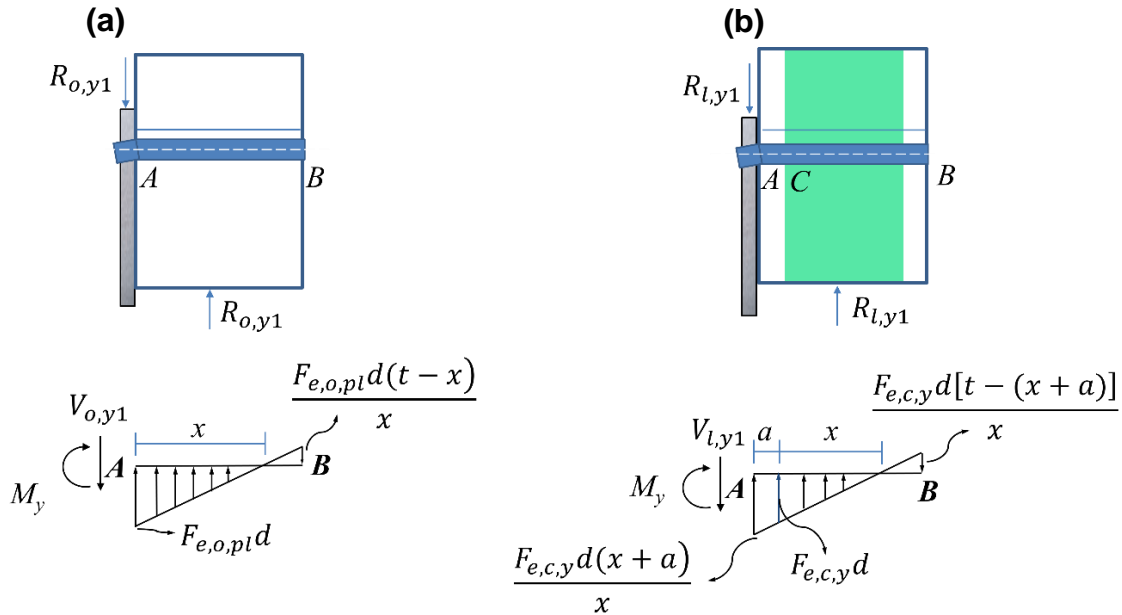


Fig. 13. Mechanical schematic diagrams for linear model (a) Model II-a and (b) Model II-b

Based on the geometric relationship of Model II-a (Fig. 13a), the bearing unit load at point B is derived as $\frac{F_{e,o,pl}d(t-x)}{x}$. Summarizing all moments to zero at pivot point A yields the following moment equation (Eq. 11).

$$M_y + \left[\frac{(t-x) \frac{F_{e,o,pl}d(t-x)}{x}}{2} \right] \left[x + \frac{2(t-x)}{3} \right] - \left(\frac{x F_{e,o,pl}d}{2} \right) \left(\frac{x}{3} \right) = 0 \quad (11)$$

Summarizing all forces in the vertical direction to zero yields the following vertical force equation (Eq. 12).

$$V_{o,y1} - \frac{1}{2} F_{e,o,pl}dx + \frac{1}{2} F_{e,o,pl}(t-x) = 0 \quad (12)$$

Solving above two equations yields the following equation for calculation of the 5% offset yield shear force at stage 1, $V_{o,y1}$ (N), at point A of the screw (Eq. 13).

$$V_{o,y1} = -\frac{1}{2} F_{e,o,pl}d \frac{2F_{e,o,pl}dt^3}{3(F_{e,o,pl}dt^3 - 2M_y)} + \frac{1}{2} F_{e,o,pl} \left(t - \frac{2F_{e,o,pl}dt^3}{3(F_{e,o,pl}dt^3 - 2M_y)} \right) \quad (13)$$

By setting $k_3 = \frac{2F_{e,o,pl}dt^3}{3(F_{e,o,pl}dt^3 - 2M_y)}$ and $R_{o,y1} = V_{o,y1}$, the lateral resistance load of SMPSCs, $R_{o,y1}$ (N), at the 5% offset yield point in Stage 1 can be estimated using the following equation based on Model II-a (Eq. 14).

$$R_{o,y1} = \frac{1}{2} F_{e,o,pl} [t + (d-1)k_3] \quad (14)$$

Based on the geometric relationship of Model II-b (Fig. 13b), the bearing unit load at point A is derived as $\frac{F_{e,c,y}d(x+a)}{x}$. The bearing unit load at point B is derived as

$\frac{F_{e,c,y}d[t-(x+a)]}{x}$. Summarizing all moments to zero at pivot point A yields the following moment equation (Eq. 15).

$$M_y + \frac{[t-(x+a)]\frac{F_{e,c,y}d[t-(x+a)]}{x}}{2} \left[(x+a) + \frac{2[t-(x+a)]}{3} \right] - \frac{(x+a)\frac{F_{e,c,y}d(x+a)}{x}}{2} \frac{x+a}{3} = 0 \quad (15)$$

Summarizing all forces in the vertical direction to zero yields the following vertical force equation (Eq. 16).

$$V_{l,y1} - \frac{1}{2} \frac{F_{e,c,y}d(x+a)}{x} (x+a) + \frac{1}{2} [t-(x+a)] \frac{F_{e,c,y}d[t-(x+a)]}{x} = 0 \quad (16)$$

Solving above two equations yields the following equation for calculation of the 5% offset yield shear force at Stage 1, $V_{l,y1}$ (N), at point A of the screw (Eq. 17).

$$V_{l,y1} = \frac{F_{e,c,y}d \left(-\frac{F_{e,c,y}dt^2(3a-2t)}{3(df t^2 - 2M_y)} + a \right)^2}{2x} - \frac{F_{e,c,y}d \left[t - \left(-\frac{F_{e,c,y}dt^2(3a-2t)}{3(df t^2 - 2M_y)} + a \right) \right]^2}{2x} \quad (17)$$

By setting $k_4 = -\frac{F_{e,c,y}dt^2(3a-2t)}{3(df t^2 - 2M_y)} + a$ and $R_{l,y1} = V_{l,y1}$, the lateral resistance load of SMPSCs, $R_{l,y1}$ (N), at the 5% offset yield point in Stage 1 can be estimated using the following equation based on Model II-b (Eq. 18).

$$R_{l,y1} = \frac{F_{e,c,y}d(2tk_4 - t^2)}{2x} \quad (18)$$

Yield models

Figure 14 shows proposed models for the derivation of prediction equations of lateral resistance loads of SMPSCs at their 5% offset yield points in Stage 2 (Fig. 10).

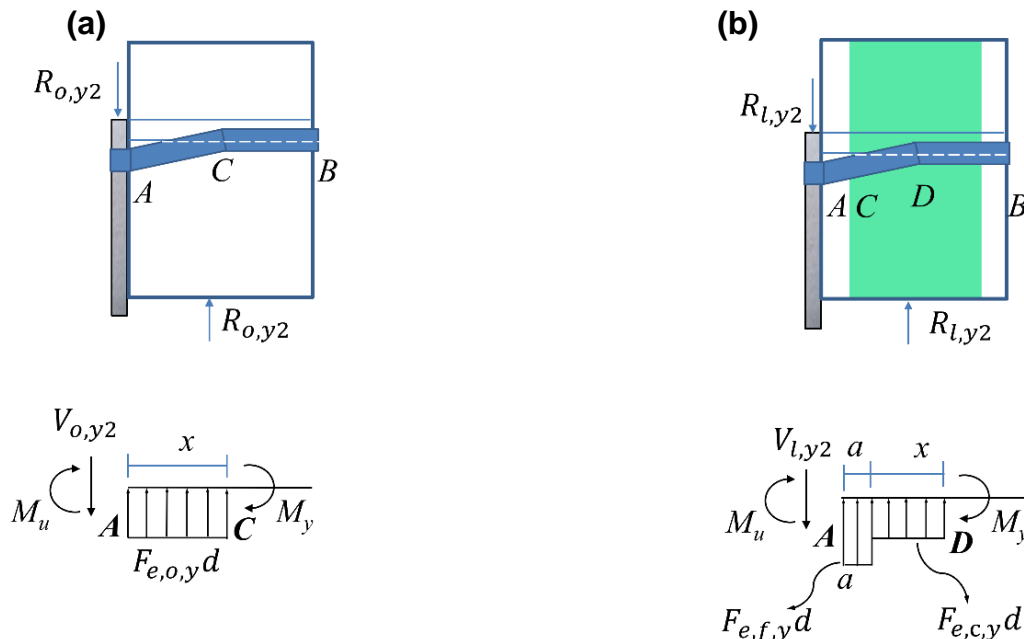


Fig. 14. Mechanical schematic diagrams for yield model (a) Model III-a, and (b) Model III-b

Specifically, Model III-a (Fig. 14a) considers PB as a uniform material across its thickness, while Model III-b (Fig. 14b) considers PB as a layered material with different screw-bearing strengths in core and face materials, respectively. The assumptions made based on the failure modes observed (Fig. 11c and d) are that 1) the compressed section of PB materials beneath the screw between two screw bent points is in its plastic deformation range and reaches to its screw-bearing strength at yield point, *i.e.*, $F_{e,o,y} d$ (N/mm) for Model III-a, and $F_{e,f,y}$ and $F_{e,c,y}$ (N/mm) for face and core materials of Model III-b respectively because of the compressive fracture of face material observed at this stage; and 3) the bending moment in the screw at the first screw bent point A reaches its ultimate point, M_u (N-mm), for both Model III-a and b, and the bending moment at the second screw bent point (C for Model III-a and D for Model III-b) reaches its yield point value, M_y (N-mm).

Based on the geometric relationship of Model III-a (Fig. 14a), summarizing all moments to zero at pivot point A yields the following moment equation (Eq. 19).

$$M_u + M_y - F_{e,o,y} d \frac{x^2}{2} = 0 \quad (19)$$

Summarizing all forces in the vertical direction to zero yields the following vertical force equation (Eq. 20).

$$V_{o,y2} - F_{e,o,y} d x = 0 \quad (20)$$

Solving above two equations yields the following equation for calculation of the 5% offset yield shear force at Stage 2, $V_{o,y2}$ (N), at point A of the screw (Eq. 21).

$$V_{o,y2} = \sqrt{2(M_u + M_y)F_{e,o,y}d} \quad (21)$$

By setting $R_{o,y2} = V_{o,y2}$, the lateral resistance load of SMPSCs, $R_{o,y2}$ (N), at the 5% offset yield point in Stage 2 can be estimated using the following equation based on Model III-a (Eq. 22).

$$R_{o,y2} = \sqrt{2(M_u + M_y)F_{e,o,y}d} \quad (22)$$

Based on the geometric relationship of Model III-b (Fig. 14b), summarizing all moments to zero at pivot point A yields the following moment equation (Eq. 23).

$$M_u + M_y - \frac{1}{2} F_{e,f,y} da^2 - F_{e,c,y} dx \left(\frac{x}{2} + a \right) = 0 \quad (23)$$

Summarizing all forces in the vertical direction to zero yields the following vertical force equation (Eq. 24).

$$V_{l,y2} = F_{e,f,y} da + F_{e,c,y} dx \quad (24)$$

Solving above two equations yields the following equation for calculation of the 5% offset yield shear force in Stage 2, $V_{l,y2}$ (N), at point A of the screw (Eq. 25).

$$V_{l,y2} = F_{e,f,y} da + \sqrt{F_{e,c,y} d (F_{e,c,y} da^2 - F_{e,f,y} da^2 + 2M_u + 2M_y)} - F_{e,c,y} da \quad (25)$$

By setting $R_{l,y2} = V_{l,y2}$, the lateral resistance load of SMPSCs, $R_{l,y2}$ (N), at the 5% offset yield point in Stage 2 can be estimated using the following equation based on Model III-b (Eq. 26).

$$R_{l,y2} = F_{e,f,y} da + \sqrt{F_{e,c,y} d (F_{e,c,y} da^2 - F_{e,f,y} da^2 + 2M_u + 2M_y)} - F_{e,c,y} da \quad (26)$$

Figure 15 shows proposed mechanical models for the derivation of prediction equations of lateral resistance loads of SMPSCs at their ultimate points in Stage 3 (Fig. 10). Specifically, Model IV-a (Fig. 15a) considers PB as a uniform material across its thickness, while Model IV-b (Fig. 15b) considers PB as a layered material with different screw-bearing strengths in core and face materials, respectively. The assumptions made based on the failure modes observed (Fig. 11e and f) are that 1) the compressed section of PB materials beneath the screw between two screw bent points is in its plastic deformation range and reaches to its screw-bearing strength at maximum point, *i.e.*, $F_{e,o,u} d$ (N/mm) for Model IV-a, and $F_{e,f,u}$ and $F_{e,c,u}$ (N/mm) for face and core materials of Model III-b respectively because of the deeper compressive crush fracture of face and core materials observed at this stage; and 3) the bending moments in the screw at both the first and second screw bent points of both Model III-a and Model III-b reach their ultimate value, M_u (N-mm).

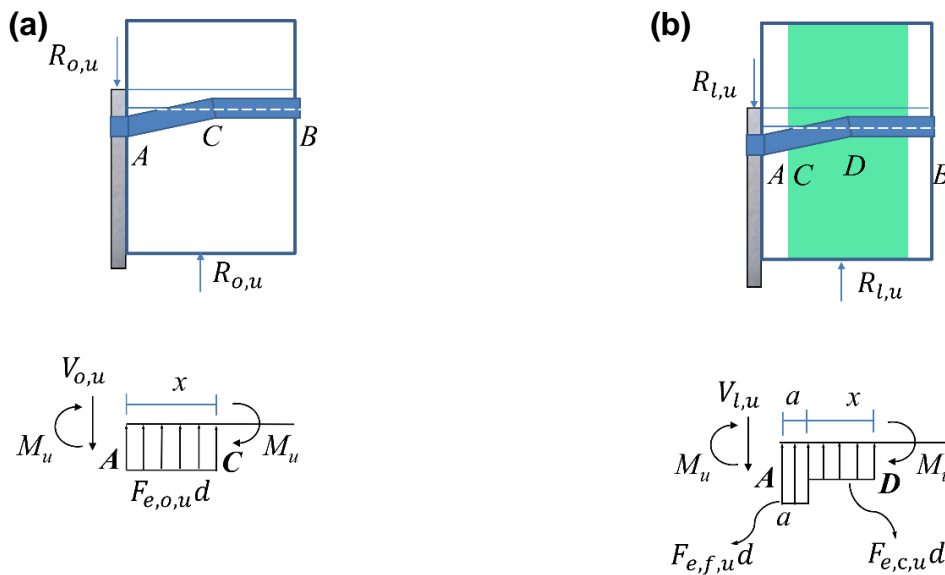


Fig. 15. Mechanical schematic diagrams for yield model (a) Model IV-a and (b) Model IV-b

Based on the geometric relationship of Model IV-a (Fig 15a), summarizing all moments to zero at pivot point A yields the following moment equation (Eq. 27).

$$2M_u - F_{e,o,u}d \frac{x^2}{2} = 0 \quad (27)$$

Summarizing all forces in the vertical direction to zero yields the following vertical force equation (Eq. 28).

$$V_{o,m} - F_{e,o,u}d x = 0 \quad (28)$$

Solving the above two equations yields the following equation for calculation of the maximum shear force at Stage 3, $V_{o,m}$ (N), at point A of the screw (Eq. 29).

$$V_{o,m} = 2\sqrt{M_u F_{e,o,u}d} \quad (29)$$

By setting $R_{o,m} = V_{o,m}$, the lateral resistance load of SMPSCs, $R_{o,m}$ (N), at maximum point in Stage 3 can be estimated using the following equation based on Model IV-a (Eq. 30).

$$R_{o,m} = 2\sqrt{M_u F_{e,o,u} d} \quad (30)$$

Based on the geometric relationship of Model IV-b (Fig 15 b), summarizing all moments to zero at pivot point A yields the following moment equation (Eq. 31).

$$2M_u - \frac{1}{2} F_{e,f,u} da^2 - F_{e,c,u} dx \left(\frac{x}{2} + a \right) = 0 \quad (31)$$

Summarizing all forces in the vertical direction to zero yields the following vertical force equation (Eq. 32).

$$V_{l,m} - F_{e,f,u} da - F_{e,c,u} dx = 0 \quad (32)$$

Solving above two equations yields the following equation for calculation of the maximum shear force at Stage 3, $V_{l,m}$ (N), for at point A of the screw (Eq. 33).

$$V_{l,m} = F_{e,f,u} da + \sqrt{F_{e,c,u} d (F_{e,c,u} da^2 - F_{e,f,u} da^2 + 4M_u)} - F_{e,c,u} da \quad (33)$$

By setting $R_{l,m} = V_{l,m}$ the lateral resistance load of SMPSCs, $R_{l,m}$ (N), at maximum point in Stage 3 can be estimated using the following equation based on Model IV-b (Eq. 34).

$$R_{l,m} = F_{e,f,u} da + \sqrt{F_{e,c,u} d (F_{e,c,u} da^2 - F_{e,f,u} da^2 + 4M_u)} - F_{e,c,u} da \quad (34)$$

Table 3 summarizes predicted values of lateral resistance loads of SMPSCs at proportional limit, yield, and ultimate points using derived prediction equations [3] through [34], and their corresponding observed values, and ratios of predicted to observed values. Ratio values of 1.42 and 1.38 for proportional limit and yield loads in stage 1, respectively, indicate that the derived prediction Eqs.1 and 3 with the consideration of PB being a uniform material across its thickness, *i.e.*, PB having a same screw-bearing strength across its thickness, tend to overestimate the lateral resistance loads of SMPSCs at their proportional limit and yield points in Stage 1. Ratio values of 0.99 and 1.02 for proportional limit and yield loads in Stage 1, respectively, indicate that the derived prediction Eqs.10 and 18 with the consideration of PB being a layered material with different screw-bearing strengths in core and face materials, respectively, can estimate the lateral resistance loads of SMPSCs at their proportional limit and yield points in Stage 1 reasonably well if compared to Eqs. 6 and 14.

Ratio values of 0.89 and 0.91 for yield loads in Stage 2 and ultimate loads in Stage 3, respectively, indicate that the derived prediction Eqs. 22 and 30 with the consideration of PB materials having an averaged screw-bearing strength across its thickness tend to underestimate the lateral resistance loads of SMPSCs at their second yield and ultimate points. Ratio values of 1.00 and 0.99 for yield loads in Stage 2 and ultimate loads, respectively, indicate that the derived prediction Eqs. 26 and 34 with the consideration of PB being a layered material with different screw-bearing strengths in core and face materials, respectively, can estimate the lateral resistance loads of SMPSCs at second yield and ultimate points reasonably well if compared to Eqs. 22 and 30. If the equation (Aune and Patton-Mallory 1986) $F_u = 1.4\sqrt{2f_e M_y}$ is used to estimate the lateral resistance load of SMPSCs at ultimate point, where: F_u is the ultimate lateral resistant load of a connection, f_e is the maximum bearing load per unit length, N/mm, M_y is the yield bending moment of a dowel connector, N-mm), with setting $f_e = F_{e,o,u} d$, the ratio of predicted to observed ultimate load is 0.88, which indicates that the equation tends to underestimate the lateral resistance load of SMPSCs at ultimate point like Eq-30.

Table 3. Lateral Resistance Predicted Equation Verifying and Comparison

	Lateral Resistance Load (N)				Predicted/Observed Ratio			
	PL in Stage 1	Yield in Stage 1	Yield in Stage 2	Maximum in Stage 3	PL in Stage 1	Yield in Stage 1	Yield in Stage 2	Maximum in Stage 3
Observed	1,726 (4.8)	1,810 (5.5)	3,910 (2.3)	4,261 (2.3)				
Aune and Patton (1986)	---	---	---	3,761	---	---	---	0.88
Uniform assumption	2,445	2,498	3,493	3,860	1.42	1.38	0.89	0.91
Non-uniform assumption	1,707	1,853	3,906	4,088	0.99	1.02	1.00	0.96

Note: Values in parentheses are coefficients of variation in percentage.

CONCLUSIONS

1. Load-slip curves of SMPSCs behave in an elastic-plastic manner. A slight yield was found in the middle of the elastic range. To study the special lateral resistance load-deformation behavior, the lateral resistance load-deformation curve was divided into three stages. The X-ray images indicated the first offset yield at the end of stage 1 was due to screw having a slight one-point bent at the interface of PB and metal plate. The second offset yield at the end of stage 2 was due to the second screw plastic hinge appeared in the inner section of the PB.
2. The mechanical models, based on the consideration of PB as a layered material with different screw-bearing strengths in core and face materials, respectively, were verified experimentally as a better means for deriving estimation equations of the lateral resistance loads of SMPSCs on critical points of their load-slip curves such as proportional limit, yield and ultimate points, if compared to the models considering PB with an averaged screw-bearing strength across its thickness.

ACKNOWLEDGMENTS

The authors acknowledge Roseburg Particleboard Company, Taylorsville, Mississippi, for providing particleboard for this study. The authors also acknowledge the support from Guizhou province science and technology supporting plan [2018]2196.

REFERENCES CITED

- ASTM D 1761 (2012). "Standard test methods for mechanical fasteners in wood," ASTM International, West Conshohocken, PA.
- ASTM D 4442 (2013). "Standard test methods for direct moisture content measurement of wood and wood-base materials," ASTM International, West Conshohocken, PA.
- ASTM D 5764 (2018). "Standard test method for evaluating dowel-bearing strength of wood and wood-based products," ASTM International, West Conshohocken, PA.
- ASTM F 1575 (2017). "Standard test method for determining bending yield moment of nails," ASTM International, West Conshohocken, PA.
- ASTM D 2395 (2017). "Standard test methods for specific gravity of wood and wood-based materials," ASTM International, West Conshohocken, PA.
- ANSI A208.1 (2016). "Particleboard," American National Standards Institute, Washington, D. C.
- Aune, P., and Patton-Mallory, M. (1986). *Lateral Load-Bearing Capacity of Nailed Joints Based on the Yield Theory: Experimental Verification (Research Paper FPL 470)*, U. S. Department of Agriculture, Forest Products Laboratory, Madison, WI.
- Blaß, H. J., and Bejtka, I. (2002). "Joints with inclined screws," International council for research and innovation in building and construction working commission w18 - timber structures. Kyoto, Japan.
- Chui, Y. H., Smith, I., and Chen, Z. (2006). "Influence of fastener size on lateral strength of steel-to-wood screw joints," *Forest Products Journal* 56, 49-54.
- Hansen, K. F. (2002). "Mechanical properties of self-tapping screws and nails in wood,"

- Canadian Journal of Civil Engineering* 29, 725-733.
- Hunt, B. R. D., and Bryant, A. H. (1990). "Laterally loaded nail joints in wood," *Journal of Structural Engineering* 116, 111-124.
- Karacabeyli, E., Fraser, H., and Deacon, W. (1998). "Lateral and withdrawal load resistance of glulam rivet connections made with sawn timber," *Canadian Journal of Civil Engineering Eng.* 25,128-138.
- Kuang, F., Wu, Z., Quin, F., and Zhang, J. (2017). "Lateral load resistance behavior of wood-plastic-to metal single-bolt connections in outdoor furniture," *Wood and Fiber Science*, 49(1), 59-72.
- Tor, O., Yu, X. H., and Zhang, J. (2015). "Characteristics of torques for driving screws into wood-based composites," *Wood and Fiber Science* 47(1), 2-16.
- Soltis, L. A., Hubbard, F. K., and Wilkinson, T. L. (1986). "Bearing strength of bolted timber joints," *Journal of Structural Engineering* 112(9), 2141-2154.
- Sinha, A, and Byrne T. M. (2013). "Lateral load carrying capacity of laminated bamboo lumber and oriented strand board connections," *Journal of Materials in Civil Engineering* 26(4), 741-747.
- Taj, M. A., Najafi, S. K., and Ebrahimi, G. (2009). "Withdrawal and lateral resistance of wood screw in beech, hornbeam and poplar," *European Journal of Wood and Wood Products* 67(2), 135-140.
- United Nations Economic Commission for Europe (UNECE) (2016). *Forest Products Annual Market Review, 2015-2016*, Geneva, Switzerland.
- Williamson, T. G. (2002). *APA Engineered Wood Handbook*, McGraw-Hill Education, New York.
- Yu, X., Dai, L., Demirel, S., Liu, H., and Zhang, J. (2017). "Lateral load resistance of parallel bamboo strand panel-to-metal single-bolt connections–part 1: Yield model," *Wood and Fiber Science* 49(4), 424-435.

Article submitted: August 10, 2018; Peer review completed: September 30, 2018;
Revised version received: October 4, 2018; Accepted: October 9, 2018; Published:
October 22, 2018.

DOI: 10.15376/biores.13.4.8911-8929